Pressure Effects and Fracture of a Rubbery Particulate Composite
by T. C. Miller and C. T. Liu

Introduction

Rubbery particulate composites used in the aerospace industry consist of a rubbery matrix with a large volume fraction of embedded rigid particles and are subjected both to long term and short term loads. Cracks may form in these composites during either storage or transport and cause catastrophic failure of the component. If we can better predict the fracture of these composites, expensive components with questionable cracks may be usable, resulting in substantial cost savings.

Research on fracture of these composites has been ongoing because of this savings potential but has been inhibited by their unique behavior. For example, the rubbery matrix material can sustain large deformations and failure is caused by growth and coalescence of voids forming around embedded particles. The large deformations and the material inhomogeneity make using conventional experimental techniques and related analytical methods difficult. Also, the viscoelasticity of the matrix requires that strain rates and temperature effects be carefully considered. These complications have slowed progress in the understanding of the fracture behavior.

Most experimental research on the fracture of rubbery particulate composites has been under ambient pressure conditions.[1-11] Under these conditions, researchers have studied the initiation of crack growth,[1,4,5,9-12] the growth rate,[2-5,8,11,13] mixed-mode cracking,[1,11,14] and crack behavior near material interfaces,[12,15-20] but the effects of pressure on these same phenomena have not been considered.

This work studies the pressure effect on a particulate composite used in aerospace applications. We tested the composite for fracture properties in a pressure chamber and investigated the initiation of crack growth and the growth rate. Various crack geometries, crack sizes, specimen geometries, and specimen thicknesses are considered. The results show that pressure elevates the fracture toughness at initiation of crack growth. Subsequent growth conforms to a power law relationship between the growth rate and the stress intensity factor. The results are consistent with previously developed results.[2-5,7,10,11,13]

Experimental Setup

The material used for the experiments was a particulate composite containing a large volume fraction (60-80%) of hard particles embedded in a rubbery matrix; Young's modulus for this composite was about 5380 kPa. Due to the nature of the matrix material, the strain rates and test temperatures for the tensile and fracture tests had to be similar. For this set of experiments, we used constant strain rates of 0.0667 mm/mm/min at room temperature (25 °C).

Figure 1 shows the dimensions for the two types of fracture specimens and Table 1 shows more testing procedure details. We tested both single edge notched tension (SENT) and surface cracked specimens. For the SENT specimens, we tested various thicknesses and crack sizes (see Fig. 1 and Table 1). The surface cracked specimens were all identical (see Fig. 1) and were tested for

comparison with the SENT specimen results. The surface cracked specimens have side cutouts to increase the relative surface area at the ends of the specimens; this prevented grip delamination before the specimen fracture. We cut the initial cracks using a razor blade for the SENT specimens and a semicircular blade for the surface cracked specimens.

Testing took place inside a pressure chamber that uses nitrogen gas to apply a pressure of 6894 kPa. The loads were applied after the temperature was stabilized. The loads are applied to grips that prevent any rotation at the specimen ends.

Table 1 — Test matrix used for pressurized fracture tests

SENT specimens		$a_0 = 2.54$ mm	$a_0 = 7.62$ mm	$a_0 = 12.70$ mm
	B = 5.08 mm	3 specimens (initiation and growth analyses)	3 specimens (initiation and growth analyses)	3 specimens (initiation and growth analyses)
	B = 12.70 mm	3 specimens (initiation and growth analyses)	3 specimens (initiation and growth analyses)	3 specimens (initiation and growth analyses)
	B = 38.10 mm	3 specimens (initiation and growth analyses)	3 specimens (initiation and growth analyses)	3 specimens (initiation and growth analyses)
Surface crack specimens	6 specimens (initiation analysis only)			

The pressure chamber has sight ports for observing the crack behavior during the test. We positioned a light at one port and a video camera at the other, so that we could observe and record the crack behavior during the test. A digital time encoder in series with the video camera and a video tape recorder imprinted times onto the videotape. We noted the time at which the test started and used this to synchronize the videotape images with the testing machine data. This procedure let us obtain the specimen displacement, load, and crack size at many times for each test.

To obtain data for the crack growth initiation, we examined the videotape to find the time at which growth began and took the loads and displacement from the synchronized data. This initiation event is detected by closely monitoring the crack tip using the video camera. At this point, the advance of the crack tip can easily be seen, and is clearly distinguishable from any previous blunting behavior. Figure 2 shows the process of blunting, damage, and growth.

Next we monitored the crack size and correlated it with loads and displacements. We measured the crack on the videotape images from the time of growth initiation until the maximum load was attained. Small apparent changes in the crack size occur before the initiation, but these are actually changes in the dimensions due to Poisson's contraction of the specimen and blunting effects, rather than due to any actual growth. We measured crack size in regular intervals that gave a reasonable

number of measurements for each test (the intervals were either one or two seconds, giving about fifteen measurements per test).

Results and Discussion

Finite Element Analysis
We used finite element results to find the stress intensities for each data point. The finite element models used eight-noded quadrilateral elements, which were degenerated into quarter-point singularity elements near the crack tip, with equivalenced nodes forming the crack tip. The elements used the hydrostatic component of stress as a variable in addition to the displacement components at each of the nodes. This type of element (*a hybrid element*) is necessary due to the incompressibility of the composite materials; the use of conventional elements results in a singular stiffness matrix and causes large errors in the results.[12,19-25] Our analysis used uniform displacement boundary conditions (to match the test conditions) and determined the J integral value with the domain integral method. The J integral value can then be converted into a stress intensity factor, K_I, using the relationship $K_I = (J E)^{1/2}$. For a given specimen, a geometric correction factor, $f(a/w)$, can be determined, so that:

$$K_I = \sigma_0 \sqrt{\pi a}\, f(a/w) \tag{1}$$

Here K_I is the stress intensity factor for a given geometry, load, and crack size, σ_0 is the remote nominal stress (load divided by gross cross sectional area), a is the crack size, and w is the specimen width. We found the geometric correction factor by determining the stress intensity factor from the finite element analysis J integral values, and then calculating the ratio $K_I/\sigma_0\sqrt{\pi a}$ for several crack sizes. A smooth polynomial curve fit of $K_I/\sigma_0\sqrt{\pi a}$ versus a/w is then used as the correction factor in eq (1). Based on finite element results for the specimens shown in Fig. 1,

$$f(a/w) = 2.694(a/w)^3 - 1.949(a/w)^2 + 1.327(a/w) + 1.008 \tag{2}$$

Because this correction factor is derived using uniform displacement boundary conditions, it differs slightly from the traditional correction factors that use traction boundary conditions. Using eqs (1) and (2), loads from the testing machine data, and crack sizes from the videotape images (at initiation of growth and during subsequent growth), the stress intensity factor during each of the SENT tests could be determined.

The surface cracked specimens were more difficult to analyze, because although the crack width (*2c* in Fig. 3) could be measured using the videotape images, the crack depth (*a*) could not. As a result, the examination of surface crack fracture phenomena was limited to determination of the stress intensity factor at the initiation of growth, when we knew both a and c. For these calculations, we used the correction factors for semielliptical surface flaws determined by Newman and Raju.[26] The correction factor in this instance depends on three ratios (*a/t*, *a/c*, and *2c/W*) as shown in Fig. 3. Based on this analysis, the stress intensity for the initial crack size shown is related to the loading through:

$$K_I = \sigma_0 \sqrt{\pi a} \ (0.6720)$$

(3)

A similar result from a simpler analysis by Irwin[27] suggests that the specimen could be analyzed as a semi-infinite plate with only crack width, depth, and specimen thickness as the governing linear dimensions.

Fracture Initiation Toughness
To explain the fracture phenomena, we must emphasize that these composites do not behave like more conventional engineering materials. The composite material can sustain much higher strains than metals (30% strains are typical), and experiences visible blunting before growth. As a specimen is stretched, increasing loads cause higher stresses near the crack tip and promote damage in front of the tip by nucleation and growth of voids from the embedded particles. At some critical point, the crack grows into this damaged region. We define the *initiation fracture toughness* as the stress intensity factor for the crack at the point when this crack growth first occurs. This event is clearly distinguishable (see Fig. 2), and was the basis for determining the initiation fracture toughness.

The overall initiation fracture toughness for the SENT specimens was determined using a regression plot. Here the nominal stress (σ_c) is plotted as the ordinate and $1/[\sqrt{\pi a_c} f(a_c/w)]$ is plotted as the abscissa (the subscripts denote the values at the critical time of growth initiation). From eq (1), the line will pass through the origin of the graph and have a slope equal to the initiation fracture toughness:

$$K_C = \frac{\sigma_c}{\dfrac{1}{\sqrt{\pi a} \ f(a/w)}}$$

(4)

Figure 4 shows this plot for the SENT specimens and also for the surface cracked specimens. This way of determining the initiation fracture toughness can be used when different crack sizes or specimen geometries are tested and shows which data points, if any, are inconsistent with the other data. Figure 4 shows that the data from the shortest of the crack sizes tested ($a_0 = 2.54$ mm) does not agree with the other results, so the short crack results are not incorporated into the least-squares curve fit of the data. For these very short cracks it is likely that a fundamental assumption inherent in linear elastic fracture mechanics has been violated (specifically, the near tip damage zone size is much smaller than in-plane dimensions such as the crack size). We used the regression plot to find the approximate size below which linear fracture mechanics cannot be used (from Fig. 4, this threshold is near 2.54 mm, but will depend on the specific materials and conditions encountered). The behavior of these short cracks has no existing fracture mechanics theories to adequately describe their behavior and requires further study.

Although we tested three distinct SENT specimen thicknesses (5.08, 12.7, and 38.1 mm), we found no significant thickness effect, and all of the fracture toughnesses were similar. This finding is consistent with previous ambient pressure testing and with damage mechanics research. This research shows that the development of damage near the crack tip prevents plane strain constraint effects so that no thickness effects are apparent.[9]

Figure 4 also shows a regression plot for the surface cracked specimens, as well as previous ambient pressure test results. The surface cracked specimens have similar K_c predictions as the SENT specimens (108.0 and 115.6 kPa √m, respectively), suggesting that the SENT specimens can be used to find the critical values for surface cracks. Furthermore, the effect of pressure is to increase the K_c value of the composite by a factor of about two. One reason for this effect may be that pressure slows the void nucleation and growth phenomena that in turn inhibits initiation of crack growth.

Crack Growth Calculations
After initiation of growth we determined the growth rate. We are interested in the growth rate because the crack may grow slowly enough to allow the component to complete its life cycle before catastrophic fracture takes place. In this case, the ability to predict the growth rate allows us to save a valuable component that otherwise would be removed from service.

Experience with rubbery particulate composites suggests that the crack growth rate is governed by a power law of the form:

$$\frac{da}{dt} = C K_I^m \tag{5}$$

Here da/dt is the crack growth rate, K_I is the stress intensity factor at some point in the crack growth history, and C and m are parameters that must be determined for a given material.[3-5,10]

We again see the distinctive behavior of the composite in the crack growth measurements, for, although eq (5) holds in the average sense, it does not accurately model the instantaneous crack speeds. This is because of the propagation mechanism: growth into a damaged region causes crack arrest, which is followed by blunting and new damage formation near the tip, resulting in more growth. The time variations in da/dt complicate the growth analysis, however, the growth rates conform to eq (5) if smoothing techniques are applied to the data before taking time derivatives.[2,3,13] We obtained crack speeds by fitting a polynomial curve to each data set and using the derivative of the polynomial evaluated at each data point as the da/dt value. Sometimes several starting or ending values of da/dt for each data set were not used in the power law fit because they gave decreasing da/dt values. This irregularity was present only in some data sets and was caused by the use of polynomial curve fitting.

We derived the power law curve that relates crack speeds to stress intensities using the aggregate data obtained from the SENT specimens (growth data was unavailable for the surface cracked specimens due to an inability to measure crack depth during testing). The parameters C and m in eq (5) can be found using a least-squares approach. As Fig. 5 shows, when we did this, we found

that $C = 7.666 \times 10^{-6}$ and $m = 1.902$ (assuming units of [mm/s] and [kPa m$^{1/2}$] for da/dt and K, respectively).

Figure 5 also shows data from previous testing under similar conditions, except ambient pressure conditions were employed. A comparison of the two data sets suggests that the pressurized environment slows crack growth, and this matches expectations based on previous work. The reasons for this retardation have not been discovered and are their investigation is recommended as a point of future study.

Conclusions

We have studied the effects of pressure on the fracture of a rubbery particulate composite. The results show that the single edge notched tension specimens can be used to find the initiation fracture toughness of surface cracks and that pressure raises the stress intensity factor at the initiation of growth. The initiation fracture toughness was determined using a regression method applied to the aggregate data, which has the advantage of showing an approximate minimum crack size for valid application of linear fracture mechanics theories. Testing multiple thicknesses of the specimens reveals that there is no significant thickness effect, a finding supported and suggested by previous work on damage evolution. Finally, a least-squares determination of a power law expression can model the rates of crack growth applied to the aggregate data. The actual growth rates are determined using the time derivatives of polynomial curve fits of the growth versus time data. Possible topics for future work include research to determine the nature and prediction of short crack growth behavior, surface crack growth rate determinations and modeling, and comparison of the rate data with ambient pressure results.

References

1.   Ravi-Chandar, K. and Liu, C. T., *Mixed-Mode Fracture of Solid Propellants*, Proceedings of the 1993 Society for Experimental Mechanics 50th Anniversary Spring Conference on Experimental Mechanics, Dearborn, Michigan, 1162-1166 (1993).
2.   Liu, C. T., *Effect of Initial Crack Length on Crack Growth*, Abstract Proceedings of Society for Experimental Mechanics Spring Conference on Experimental Mechanics, Bellevue, Washington, 220-221 (1997).
3.   Liu, C. T., *The Effect of Micro Damage on Time-Dependent Crack Growth in a Composite Solid Propellant*, Mechanics of Time-Dependent Materials, **1**, 123-136 (1997).
4.   Baron, D., Miller, T. C. and Liu, C. T., *Subcritical Crack Growth in a Composite Solid Propellant*, Proceedings of the 1998 Annual Spring Conference of the Society for Experimental Mechanics, Houston, Texas, 38-39 (1998).
5.   Baron, D. T., Miller, T. C. and Liu, C. T., *Subcritical Crack Growth in a Composite Solid Propellant*, Journal of Reinforced Polymer Composites, **18**(3), 233-250 (1999).
6.   Liu, C. T., *Effects of Microstructure on Damage Evolution, Strain Inhomogeneity, and Fracture in a Particulate Composite*, International Conference on Recent Development in Durability Analysis of a Composite System, Brussels, Belgium, (1999).
7.   Liu, C. T., *Predicting Crack Growth Behavior in a Filled Polymeric Material*, ASME Summer Conference on Mechanics and Materials, Blacksburg, Virginia, 27 (1999).

8.   Liu, C. T. and Gonzalez, J., *Microstructure Induced Inhomogeneous Strain in a Particulate Composite*, ASME Summer Conference on Mechanics and Materials, Blacksburg, Virginia, 37 (1999).

9.   Liu, C. T. and Miller, T. C., *Effect of Near Tip Damage on the Initiation Fracture Toughness of a Particulate Composite*, ASME Summer Conference on Mechanics and Materials, Symposium on Experiments in Fracture Mechanics, Blacksburg, Virginia, 69 (1999).

10.   Miller, T. C., *Mixed-Mode Fracture in a Rubbery Particulate Composite*, Sixth International Conference on Composites Engineering, Orlando, Florida, 575-576 (1999).

11.   Miller, T. C., *Analysis of Mixed-Mode Cracks in a Rubbery Particulate Composite*, Composites Part B: Engineering, , (2000) (to be published).

12.   Miller, T. C., *Mode Mixity Determinations for Interfacial Cracking in Incompressible Materials Under Plane Strain Conditions*, International Conference on Computational Engineering Science, Atlanta, Georgia, 1323-1328 (1998).

13.   Liu, C. T., *Critical Analysis of Crack Growth Data*, Journal of Propulsion, **6**(5), 519-524 (1990).

14.   Miller, T. C., *An Experimental Investigation of a Thermally Loaded Interfacial Crack*, Proceedings of the 1997 Annual Spring Conference of the Society for Experimental Mechanics, Bellevue, Washington, 241-242 (June 1997).

15.   Bowen, J. M. and Knauss, W. G., *The Characterization of the Energy of Fracture at or near Interfaces Between Viscoelastic Solids*, Journal of Adhesion, **39**, 1-17 (1992).

16.   Bowen, J. M. and Knauss, W. G., *An Experimental Study of Interfacial Crack Kinking*, Experimental Mechanics, **33**, 37-43 (1993).

17.   Geubelle, P. H., *Nonlinear Effects in Interfacial Fracture*, Ph.D. Dissertation, California Institute of Technology, Pasadena, California (1993).

18.   Smith, C. W., Finlayson, E. F. and Liu, C. T., *A Method for Evaluating Stress Intensity Distribution for Cracks in Rocket Motor Bondlines*, Engineering Fracture Mechanics, **58**, 97-105 (1997).

19.   Miller, T. C., *Adhesive Layer Effects on Interfacial Crack Tip Asymptotic Fields*, Fifth International Conference on Composites Engineering, Las Vegas, Nevada, 617-618 (1998).

20.   Miller, T. C., *Modelling of Plane Strain Interfacial Fracture in Incompressible Materials*, Composites Part B: Engineering, **30**(3), 291-296 (1999).\

21.   Cook, R. D., Malkus, D. S. and Plesha, M. E., Concepts and Applications of Finite Element Analysis, 3rd ed., Wiley & Sons, New York (1989).

22.   ABAQUS/Standard User's Manual, Version 5.5, Hibbitt, Karlsson, and Sorenson, Pawtucket, Rhode Island (1995).

23.   ABAQUS Theory Manual, Version 5.5, Hibbitt, Karlsson, and Sorenson, Pawtucket, Rhode Island (1995).

24.   Bathe, K.-J., Finite Element Procedures, Prentice-Hall, Upper Saddle River, New Jersey (1996).

25.   Miller, T. C., *Modeling of Interfacial Fracture in Photoelastic Specimens*, Proceedings of the 1998 Annual Spring Conference of the Society for Experimental Mechanics, Houston, Texas, 245-247 (1998).

26.   Newman, J. C., Jr., *A Review and Assessment of the Stress-Intensity Factors for Surface Cracks*, in Special Technical Publication 687: Part-Through Crack Fatigue Life Prediction, J. B. Chang, ed., American Society for Testing and Materials, 16-42 (1979).

27.   Irwin, G. R., *Crack Extension Force for a Part Through Crack in a Plate*, Journal of Applied Mechanics, **29**(4), 651-654 (1962).

List of Captions

Fig. 1 — Specimens used in pressurized fracture tests

Fig. 2 — Progression of crack growth in a rubbery particulate composite

Fig. 3 — Nomenclature for surface crack correction factors

Fig. 4 — Regression plots for finding initiation fracture toughness. The solid line shows the trend for the single edge notched (SENT) specimens, the dashed line for surface cracked specimens, and the dotted line for previous tests at ambient pressure.

Fig. 5 — Determination of crack growth law using aggregate of single edge notched tension specimen data
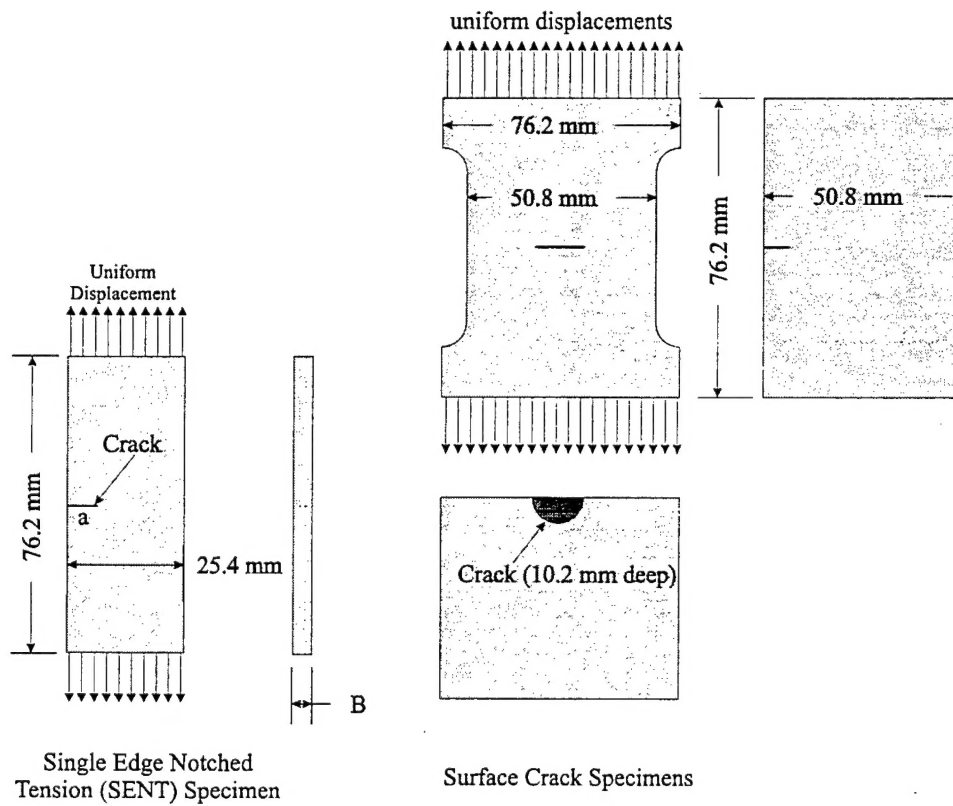
Fig. 1
Timothy Miller

uniform displacements

76.2 mm

50.8 mm

76.2 mm

50.8 mm

Crack (10.2 mm deep)

Surface Crack Specimens

Uniform
Displacement

Crack

a

76.2 mm

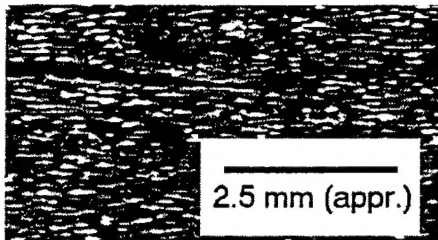25.4 mm

B

Single Edge Notched
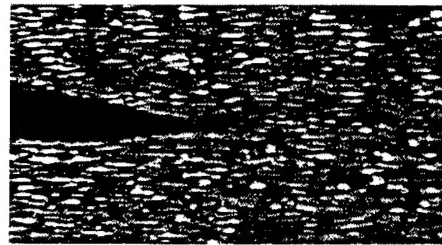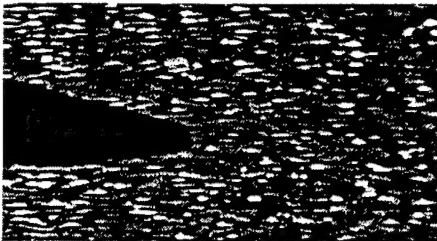Tension (SENT) Specimen
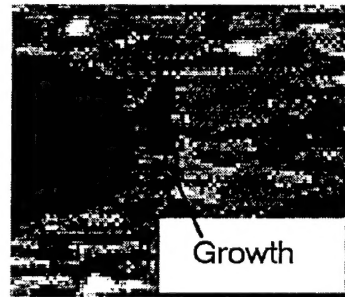
Fig. 2
Timothy Miller

a) Start of growth (sharp crack)

b) Continued loading

c) Continued blunting of crack tip

d) Initiation of crack growth at blunted crack tip

e) Continued growth
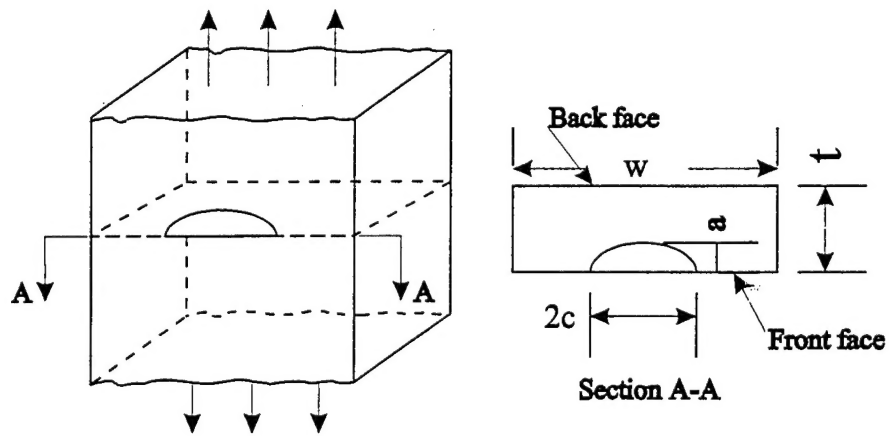
f) Further growth

Fig. 3
Timothy Miller

Back face

w

t
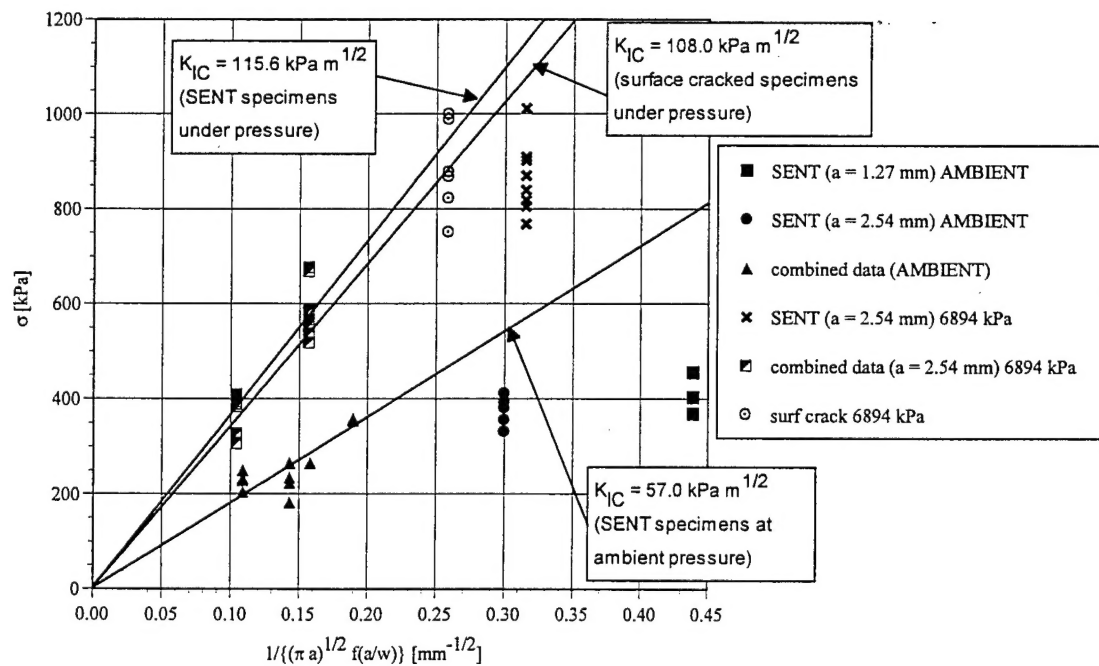
2c

a

Front face

Section A-A

Fig. 4
Timothy Miller

$K_{IC} = 115.6$ kPa m$^{1/2}$
(SENT specimens
under pressure)

$K_{IC} = 108.0$ kPa m$^{1/2}$
(surface cracked specimens
under pressure)

1200

1000

800

σ [kPa]

600

400

200

0

■ SENT (a = 1.27 mm) AMBIENT

● SENT (a = 2.54 mm) AMBIENT

▲ combined data (AMBIENT)

✕ SENT (a = 2.54 mm) 6894 kPa

▨ combined data (a = 2.54 mm) 6894 kPa

⊙ surf crack 6894 kPa

$K_{IC} = 57.0$ kPa m$^{1/2}$
(SENT specimens at
ambient pressure)

0.00   0.05   0.10   0.15   0.20   0.25   0.30   0.35   0.40   0.45

$1/\{(\pi a)^{1/2} f(a/w)\}$ [mm$^{-1/2}$]

Fig. 5
Timothy Miller

AMBIENT PRESSURE DATA

$da/dt = CK^m$
$C = 1.9274E-5, m = 2.088$

PRESSURIZED DATA

$da/dt = CK^m$
$C = 7.666E-6, m = 1.902$

da/dt [mm/s]

K [kPa m$^{1/2}$]